Coupled Systems Mechanics, *Vol. 14, No. 1 (2025) 87-103*
https://doi.org/10.12989/csm.2025.14.1.087

Thermal buckling analysis of new functionally graded cylindrical shells

Abbes Ouadah[1], Ahmed Draï[2,3], Ahmed Amine Daikh[4], Noureddine Boualem[1], Tarek Merzouki[5], Mohamed Oudjedi Belarbi[6,7], Mohammed Sid Ahmed Houari*[8] and M.A. Eltaher[9,10]

[1]Laboratory of Composites Structures and Innovative Materials (LCSIM), Mechanical Engineering Faculty, USTO-MB Oran, P.O. Box 1505 El- M'Naouer, Oran, Algeria
[2]Mechanical Engineering Department, Faculty of Sciences and Technology, Mustapha Stambouli University of Mascara, 29000, Algeria
[3]Laboratory of Applied Biomechanics and Biomaterials (LABAB), ENPO, Oran, 31000, Algeria
[4]Artificial Intelligence Laboratory for Mechanical and Civil Structures, and Soil, University Centre of Naama, P.O. Box 66, Naama 45000, Algeria
[5]LISV, University of Versailles Saint-Quentin, 10-12 Avenue de l'Europe, 78140 Vélizy, France
[6]Laboratoire de Recherche en Génie Civil, LRGC, Université de Biskra, B.P. 145, R.P. 07000, Biskra, Algeria
[7]Department of Civil Engineering, Lebanese American University, Byblos, Lebanon
[8]Laboratoire d'Etude des Structures et de Mécanique des Matériaux, Département de Génie Civil, Faculté des Sciences et de la Technologie, Université Mustapha Stambouli B.P. 305, R.P. 29000 Mascara, Algérie
[9]Faculty of Engineering, Mechanical Engineering Department, King Abdulaziz University, P.O. Box 80204, Jeddah, Saudi Arabia
[10]Faculty of Engineering, Mechanical Design and Production Department, Zagazig University, P.O. Box 44519, Zagazig, Egypt

(Received October 25, 2024, Revised March 23, 2025, Accepted March 23, 2025)

Abstract. This study investigates the thermal buckling behavior of novel functionally graded (FG) cylindrical shell, where material properties and thermal expansion coefficients vary continuously across the thickness using two newly introduced cosine functions, FG-A and FG-B. Equilibrium and stability equations for FG cylindrical pipes with simply supported boundary conditions are derived using Donnell's theory. The research examines how the geometric characteristics of cylindrical pipes and the inhomogeneity parameter (gradient index) collectively influence the critical buckling temperature of various functionally graded cylindrical structures. Thermal loads are assumed to vary uniformly, linearly, or nonlinearly across the thickness, with exact and simplified formulations provided for each temperature rise scenario.

Keywords: Donnell's theory; new FG cosine functions; thermal buckling; thermal loads

*Corresponding author, Ph.D., E-mail: ms.houari@univ-mascara.dz

http://www.techno-press.org/?journal=csm&subpage=8 ISSN: 2234-2184 (Print), 2234-2192 (Online)

1. Introduction

In engineering materials science, Functionally Graded Materials (FGMs) represent a significant advancement due to their unique composition, which varies gradually throughout the material. This gradation allows for tailored mechanical, thermal, and chemical properties, enabling FGMs to perform exceptionally well in extreme environments (Elmascri *et al.* 2020, Bezzina *et al.* 2022, Daikh *et al.* 2023, Wei *et al.* 2024, Belarbi *et al.* 2025, Mokhefi *et al.* 2024, Daikh *et al.* 2022, Daikh *et al.* 2024). Their applications are diverse, including aerospace components requiring high strength-to-weight ratios, biomedical implants that closely mimic natural bone properties, automotive parts designed to withstand severe thermal and mechanical stresses, and electronic substrates optimized for thermal management. The adaptability and performance enhancement provided by FGMs make them a pivotal innovation in modern engineering, addressing challenges across multiple industries.

Studying buckling behavior is crucial in engineering and structural design, as it directly impacts the safety and reliability of structures such as columns and beams. Buckling can lead to sudden failures, making it essential to understand the factors that influence it, such as material properties and loading conditions. This knowledge allows engineers to design safer and more efficient structures, optimizing material use while minimizing weight and maintaining strength. Furthermore, insights from buckling studies contribute to the development of advanced materials and systems, enhancing performance under various loading conditions. Overall, understanding buckling is vital for ensuring structural integrity and fostering innovation in engineering.

Bhangale *et al.* (2006) conducted a linear thermoelastic thermal buckling analysis of FGM conical shells, considering temperature-dependent material properties and using a semi-analytical finite element method to evaluate the thermal buckling temperature. Lanhe *et al.* (2007) analyzed the dynamic stability of thick FGM plates subjected to aero-thermomechanical loads using a novel numerical method. Their study explored the influence of various factors, such as gradient index and boundary conditions, on dynamic instability. Shen (2009) presented a thermal post-buckling analysis of a simply supported, shear-deformable FGM plate under thermal loading. The study examined the effects of temperature dependency and volume fraction index on the thermal post-buckling behavior of shear-deformable FGM plates. The governing equations were based on a higher-order shear deformation plate theory, incorporating thermal effects. The initial geometric imperfection of the plate was also considered. Results demonstrated that temperature dependency significantly affects the thermal post-buckling behavior of FGM plates.

Sofiyev *et al.* (2009) investigated the buckling of FGM hybrid truncated conical shells subjected to non-uniform lateral pressure. Detailed parametric studies were conducted to examine the effects of the radius-to-thickness ratio, length-to-radius ratio, and material composition on the critical parameters of three-layered truncated conical shells. Oyekoya *et al.* (2009) analyzed the vibration and buckling of functionally graded composite plates, optimizing fiber distributions to maximize vibration frequency and buckling load. Park and Kim (2006) investigated the thermal post-buckling and vibration behaviors of FGM plates using nonlinear finite element analysis, highlighting the influence of volume fraction on thermal post-buckling and vibration characteristics.

Shen (2007) studied the torsional buckling and post-buckling of FGM cylindrical shells in thermal environments, accounting for both heat conduction and temperature-dependent material properties. Sofiyev *et al.* (2010) analyzed the stability of truncated FGM conical shells subjected to non-uniform lateral pressure, exploring the influence of material property variations and geometric parameters on critical buckling loads and fundamental frequencies. Sofiyev *et al.* (2008) also examined the vibration and stability of freely supported FGM truncated and complete conical shells subjected to uniform lateral and hydrostatic pressures. The effects of conical shell characteristics and material composition profiles on buckling pressures and fundamental frequencies were studied.

Sepiani *et al.* (2010) investigated the free vibration and buckling of two-layered FGM cylindrical shells under combined static and periodic axial forces. The study incorporated temperature-dependent material properties and employed both first-order shear deformation theory (FSDT) and classical shell theory (CST). Sofiyev (2009) examined the buckling behavior of FGM truncated conical shells resting on elastic foundations under axial compression, considering the effects of different FGM property distributions and foundation parameters. Nejad *et al.* (2010) reviewed critical issues in the development of thick shells made from functionally graded piezoelectric materials (FGPM), focusing on various analysis methods, including plane elasticity, shear deformation, and shell theories.

Farhatnia *et al.* (2010) performed a thermal buckling analysis of an orthotropic FGM circular plate resting on a Pasternak elastic foundation. Čukanović *et al.* (2010) conducted a thermal buckling analysis of functionally graded thick rectangular plates using von Karman nonlinear theory. Zhang *et al.* (2010) analyzed the dynamic buckling of FGM cylindrical shells under thermal shock using an analytical method. Chen *et al.* (2010) investigated the thermal buckling behavior of Euler-Bernoulli FGM beams, discussing the effects of material composition, temperature-dependent material properties, slenderness ratios, and boundary conditions on thermal buckling behavior. Results revealed that these parameters significantly influence the thermal buckling characteristics of FG beams.

Radaković *et al.* (2010) studied the thermal buckling and free vibration of functionally graded square and rectangular plates of varying thicknesses resting on an elastic foundation modeled using Winkler-Pasternak theory. An analytical method was developed to determine natural frequencies and critical buckling temperatures for both linear and nonlinear temperature variations through the plate thickness. Equilibrium and stability equations were derived using higher-order shear deformation theory, incorporating various shape functions and von Karman nonlinearity.

Mohammadi *et al.* (2010) provided an overview of FGM classifications, manufacturing processes, and applications. Li *et al.* (2010) presented an analytical solution for the thermomechanical buckling of FGM sandwich plates using a four-variable equivalent single-layer (ESL) plate theory, investigating the effects of volume fraction distribution and geometric parameters. A linear relationship between mechanical load and temperature increment was established for buckling.

Do *et al.* (2010) developed a finite element model coupled with phase-field theory for the static buckling of cracked FGM plates under thermal loading. Phase-field theory was employed as a novel approach to fracture problems. The model was based on third-order shear deformation theory, considering both temperature-dependent and independent material properties. Numerical results highlighted the influence of gradient index, crack length, crack angle, and thickness on thermal buckling behavior under three boundary conditions.

Anil Kumar Gupta and Ajay Kumar (2010) investigated the buckling behavior of porous functionally graded material (PFGM) plates. Their model assumed unevenly distributed porosity and employed novel hyperbolic shear deformation functions as well as hyperbolic tangent and secant thickness stretching functions. Parametric studies examined the effect of porosity on buckling behavior with varying side-to-thickness ratios.

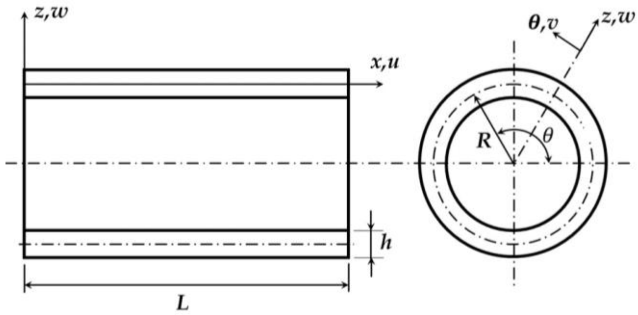

Fig. 1 Configuration and coordinate system of cylindrical pipe

Maknun and Annisa (2010) performed a thermomechanical buckling analysis of square FGM plates using a numerical evaluation to determine critical load or critical temperature. Three triangular elements (DKMT, DST, and MITC3) were employed, demonstrating accurate results for square FGM plate problems. Ngo *et al.* (2010) focused on nonlinear instability problems, addressing both geometric instability at large displacements and material instability due to softening under combined thermomechanical loads. Their work provided a comprehensive theoretical formulation, discrete approximation, and solution algorithm for such complex scenarios.

Ibrahimbegovic *et al.* (2010) proposed a novel procedure for the direct computation of buckling loads under extreme mechanical or thermomechanical conditions, utilizing the von Kármán strain measure to develop a general linear eigenvalue problem for critical load multiplier estimates.

This study focuses on the thermal buckling behavior of simply supported functionally graded cylindrical pipes, categorized as FG-A and FG-B. A simplified form is proposed for the nonlinear temperature distribution through the thickness, considering both thermal conductivity and the inhomogeneity parameter. Material properties, such as the coefficient of thermal expansion and Young's modulus, are assumed to vary continuously through the thickness according to a cosine sigmoid function. The equilibrium equations for the functionally graded cylindrical shell are derived based on Donnell's theory.

2. Functionally graded cylindrical pipes

Consider a functionally graded cylindrical pipe made of three layers of arbitrary thickness h, mid-surface radius R and length L as shown in Fig. 1. We use cylindrical coordinates with the origin located at the mid-surface of the cylinder, and coordinates x, θ, and z in the axial, the circumferential, and the thickness directions, respectively. The inner and outer faces of the cylindrical shell are at $z = \pm h/2$.

The material characteristics of the two types of new FG cylindrical pipes that have been proposed, FG-A and FG-B, are supposed to vary continuously through-thickness and are affected by a variety of variables, including temperature and porosity. The effective material properties, like Young's modulus E, and Poisson's ratio ν, can be mathematically expressed by the rule of the mixture (see Fig. 2)

$$P^{(n)}(z) = P_m + (P_c - P_m)V^{(n)}(z) \tag{1}$$

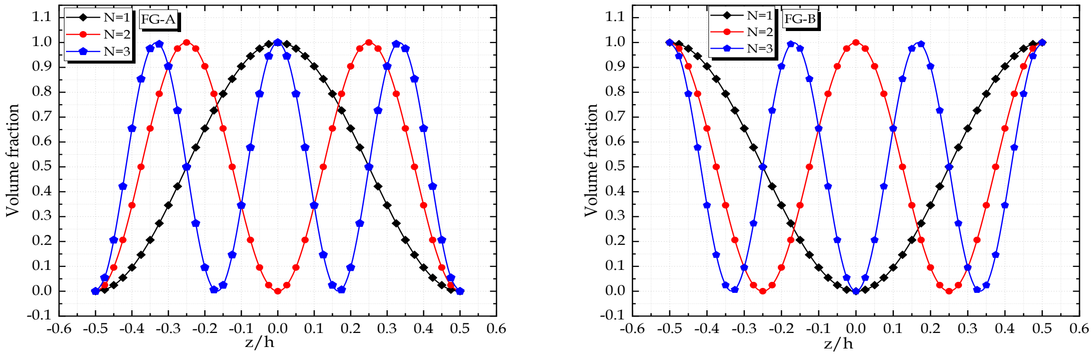

Fig. 2 Variation of volume fraction across the thickness (*z/h*) for different values of the inhomogeneity parameter (*N*=1, 2, 3)

Metal and ceramic components are indicated by the subscripts *m* and *c*, respectively.
The effective volume fraction is given as:

- For the FG-A cylindrical pipe:

$$V(z) = \frac{1}{2}\left[1 + \cos\left(N\frac{2\pi z}{h}\right)\right] \tag{2}$$

- For the FG-B cylindrical pipe:

$$V(z) = \frac{1}{2}\left[1 - \cos\left(N\frac{2\pi z}{h}\right)\right] \tag{3}$$

Here, "*N*" presents the material's inhomogeneity number.

3. Mathematical formulation

Consider a cylindrical pipe of mean radius *R* and thickness *h* with length *L* (Fig. 1). The normal and shear strains at distance *z* from the shell middle surface based on the Donnell shell theory are

$$\begin{aligned} \varepsilon_x &= \varepsilon_x^0 + z\kappa_x \\ \varepsilon_\theta &= \varepsilon_\theta^0 + z\kappa_\theta \\ \gamma_{x\theta} &= \gamma_{x\theta}^0 + z\kappa_{x\theta} \end{aligned} \tag{4}$$

Where

$$\begin{gathered} \varepsilon_x^0 = \frac{\partial u}{\partial x} + \frac{1}{2}\frac{\partial w^2}{\partial x}, \quad \varepsilon_\theta^0 = \frac{1}{R}\left(\frac{\partial v}{\partial \theta} + w\right) + \frac{1}{2R^2}\left(v - \frac{\partial w}{\partial \theta}\right)^2 \\ \gamma_{x\theta}^0 = \frac{\partial v}{\partial x} + \frac{1}{R}\frac{\partial u}{\partial \theta} + \frac{1}{R}\frac{\partial w}{\partial x}\left(\frac{\partial w}{\partial \theta} - v\right) \\ \kappa_x = -\frac{\partial^2 w}{\partial x^2}, \qquad \kappa_\theta = -\frac{1}{R^2}\frac{\partial^2 w}{\partial \theta^2}, \qquad \kappa_{x\theta} = -\frac{2}{R}\frac{\partial^2 w}{\partial x \partial \theta} \end{gathered} \tag{5}$$

Where *u*, *v*, and *w* denote the axial, circumferential, and lateral displacements of the cylindrical shell, respectively. The constitutive relations of the cylindrical pipe can be written as

$$\begin{Bmatrix} \sigma_x \\ \sigma_\theta \\ \tau_{x\theta} \end{Bmatrix} = \begin{bmatrix} Q_{11} & Q_{12} & 0 \\ Q_{12} & Q_{22} & 0 \\ 0 & 0 & Q_{66} \end{bmatrix} \begin{Bmatrix} \varepsilon_x \\ \varepsilon_\theta \\ \gamma_{x\theta} \end{Bmatrix} - \frac{E(z)\alpha(z)T}{(1-\upsilon)} \begin{Bmatrix} 1 \\ 1 \\ 0 \end{Bmatrix} \tag{6}$$

Where

$$Q_{11} = Q_{22} = \frac{E(z)}{1-\upsilon^2}, Q_{12} = \upsilon Q_{11}, Q_{66} = \frac{E(z)}{2(1+\upsilon)} \tag{7}$$

and T (z) is the temperature rise through the thickness. The membrane forces and bending moments per unit length expressed in terms of the stress as

$$\begin{gathered}\begin{Bmatrix} N_x \\ N_\theta \\ N_{x\theta} \end{Bmatrix} = \int_{-h/2}^{h/2} \begin{Bmatrix} \sigma_x \\ \sigma_\theta \\ \tau_{x\theta} \end{Bmatrix} dz \\ \begin{Bmatrix} M_x \\ M_\theta \\ M_{x\theta} \end{Bmatrix} = \int_{-h/2}^{h/2} \begin{Bmatrix} \sigma_x \\ \sigma_\theta \\ \tau_{x\theta} \end{Bmatrix} zdz\end{gathered} \tag{8}$$

By substituting (4) and (6) into (8), the stress resultants of a cylindrical shell are related to the strains by the relations

$$\begin{Bmatrix} N_x \\ N_\theta \\ N_{x\theta} \\ M_x \\ M_\theta \\ M_{x\theta} \end{Bmatrix} = \begin{bmatrix} A_{11} & A_{12} & 0 & B_{11} & B_{12} & 0 \\ A_{21} & A_{22} & 0 & B_{12} & B_{22} & 0 \\ 0 & 0 & Q_{11} & 0 & 0 & Q_{22} \\ B_{11} & B_{12} & 0 & D_{11} & D_{12} & 0 \\ B_{21} & B_{22} & 0 & D_{12} & D_{22} & 0 \\ 0 & 0 & Q_{22} & 0 & 0 & Q_{33} \end{bmatrix} \begin{Bmatrix} \varepsilon_x^0 \\ \varepsilon_\theta^0 \\ \gamma_{x\theta}^0 \\ k_x \\ k_\theta \\ k_{x\theta} \end{Bmatrix} - \begin{Bmatrix} N_T \\ N_T \\ 0 \\ M_T \\ M_T \\ 0 \end{Bmatrix} \tag{9}$$

Where

$$\{A_{11}, B_{11}, D_{11}\} = \int_{-\frac{h}{2}}^{\frac{h}{2}} \{1, z, z^2\} \frac{E}{1-\upsilon^2} \mathrm{d}z, \ \{A_{12}, B_{12}, D_{12}\} = \int_{-\frac{h}{2}}^{\frac{h}{2}} \{1, z, z^2\} \frac{\upsilon E}{1-\upsilon^2} \mathrm{d}z, \{Q_{11}, Q_{22}, Q_{33}\} = \int_{-\frac{h}{2}}^{\frac{h}{2}} \{1, z, z^2\} \frac{E}{2(1+\upsilon)} \mathrm{d}z \tag{10}$$

and $\{N^T\}, \{M^T\}$ temperature-induced forces

$$\{N_T, M_T\} = \int_{-\frac{h}{2}}^{\frac{h}{2}} \{1, z\}\{\beta\} T \mathrm{d}z \tag{11}$$

Where

$$\{\beta\} = \{(Q_{11} + Q_{12})\alpha(z), (Q_{12} + Q_{22})\alpha(z)\} \tag{12}$$

4. Stability equations

By using Donnell shell theory, the equilibrium equations for general thin cylindrical pipe are obtained as

$$\begin{gathered}\frac{\partial N_x}{\partial x} + \frac{1}{R}\frac{\partial N_{x\theta}}{\partial \theta} = 0 \\ \frac{1}{R}\frac{\partial N_\theta}{\partial \theta} + \frac{\partial N_{x\theta}}{\partial x} = 0 \\ \frac{\partial^2 M_x}{\partial x^2} + \frac{2}{R}\frac{\partial^2 M_{x\theta}}{\partial x \partial \theta} + \frac{1}{R^2}\frac{\partial^2 M_\theta}{\partial \theta^2} - \frac{1}{R} N_\theta + N_x \frac{\partial^2 w}{\partial x^2} + \frac{1}{R^2} N_\theta \frac{\partial^2 w}{\partial \theta^2} + \frac{2}{R} N_{x\theta} \frac{\partial^2 w}{\partial x \partial \theta} = 0\end{gathered} \tag{13}$$

Assuming that the equilibrium state of the cylindrical pipe under thermal loads may be designated by u^0, v^0, w^0. The displacement components of a neighboring stable state differ by u^1, v^1, w^1 with respect to the equilibrium position. The displacements of a neighboring state are

$$u = u^0 + u^1, v = v^0 + v^1, w = w^0 + w^1 \tag{14}$$

The terms with subscripts 0 refer to the state of equilibrium conditions, and the terms with subscripts 1 refer to the state of stability. Note that whereas the equilibrium equations are nonlinear, the stability equations are linear. The linearised strains and curvatures in terms of the displacement component are

$$\begin{aligned}
&{\varepsilon_x^0}^1 = \frac{\partial u^1}{\partial x}, \qquad {\varepsilon_\theta^0}^1 = \frac{1}{R}\left(\frac{\partial v^1}{\partial \theta} + w^1\right), \quad {\gamma_{x\theta}^0}^1 = \frac{\partial v^1}{\partial x} + \frac{1}{R}\frac{\partial u^1}{\partial \theta} \\
&{\kappa_x}^1 = -\frac{\partial^2 w^1}{\partial x^2}, \qquad {\kappa_\theta}^1 = -\frac{1}{R^2}\frac{\partial^2 w^1}{\partial \theta^2} \qquad {\kappa_{x\theta}}^1 = -\frac{1}{R}\frac{\partial^2 w^1}{\partial x \partial \theta}
\end{aligned} \tag{15}$$

The stress and moment resultants may be related to the equilibrium and neighbouring states as

$$\begin{aligned}
N_x &= N_x^0 + N_x^1, \quad N_\theta = N_\theta^0 + N_\theta^1, \quad N_{x\theta} = N_{x\theta}^0 + N_{x\theta}^1 \\
M_x &= M_x^0 + M_x^1, \quad M_\theta = M_\theta^0 + M_\theta^1, \quad M_{x\theta} = M_{x\theta}^0 + M_{x\theta}^1
\end{aligned} \tag{16}$$

Eliminating the pre-buckling equilibrium expressions and ignoring the nonlinear terms of the incremental variables, we obtain the governing equations for buckling according to the Donnell theory as follows

$$\begin{gathered}
\frac{\partial N_x^1}{\partial x} + \frac{1}{R}\frac{\partial N_{x\theta}^1}{\partial \theta} = 0 \\
\frac{1}{R}\frac{\partial N_\theta^1}{\partial \theta} + \frac{\partial N_{x\theta}^1}{\partial x} = 0 \\
\frac{\partial^2 M_x^1}{\partial x^2} + \frac{2}{R}\frac{\partial^2 M_{x\theta}^1}{\partial x \partial \theta} + \frac{1}{R^2}\frac{\partial^2 M_\theta^1}{\partial \theta^2} - \frac{1}{R}N_\theta^1 + N_x^0\frac{\partial^2 w^1}{\partial x^2} + \frac{1}{R^2}N_\theta^0\frac{\partial^2 w^1}{\partial \theta^2} + \frac{2}{R}N_{x\theta}^0\frac{\partial^2 w^1}{\partial x \partial \theta} = 0
\end{gathered} \tag{17}$$

Where

$$\begin{gathered}
N_x^0 = -N_T \\
N_\theta^0 = N_{x\theta}^0 = 0
\end{gathered} \tag{18}$$

The forces and moments associated with the stability state are

$$\begin{aligned}
N_x^1 &= A_{11}\frac{\partial u^1}{\partial x} + \frac{A_{12}}{R}\left(w^1 + \frac{\partial v^1}{\partial \theta}\right) - B_{11}\frac{\partial^2 w^1}{\partial x^2} - \frac{B_{12}}{R^2}\frac{\partial^2 w^1}{\partial \theta^2} \\
N_\theta^1 &= A_{12}\frac{\partial u^1}{\partial x} + \frac{A_{11}}{R}\left(w^1 + \frac{\partial v^1}{\partial \theta}\right) - \frac{B_{11}}{R^2}\frac{\partial^2 w^1}{\partial \theta^2} - B_{12}\frac{\partial^2 w^1}{\partial x^2} \\
N_{x\theta}^1 &= Q_{11}\left(\frac{\partial v^1}{\partial x} + \frac{1}{R}\frac{\partial u^1}{\partial \theta}\right) - \frac{2Q_{22}}{R}\frac{\partial^2 w^1}{\partial x \partial \theta} \\
M_x^1 &= B_{11}\frac{\partial u^1}{\partial x} + \frac{B_{12}}{R}\left(w^1 + \frac{\partial v^1}{\partial \theta}\right) - D_{11}\frac{\partial^2 w^1}{\partial x^2} - \frac{D_{12}}{R^2}\frac{\partial^2 w^1}{\partial \theta^2} \\
M_\theta^1 &= B_{12}\frac{\partial u^1}{\partial x} + \frac{B_{11}}{R}\left(w^1 + \frac{\partial v^1}{\partial \theta}\right) - \frac{D_{11}}{R^2}\frac{\partial^2 w^1}{\partial \theta^2} - D_{12}\frac{\partial^2 w^1}{\partial x^2} \\
M_{x\theta}^1 &= Q_{22}\left(\frac{\partial v^1}{\partial x} + \frac{1}{R}\frac{\partial u^1}{\partial \theta}\right) - \frac{2Q_{33}}{R}\frac{\partial^2 w^1}{\partial x \partial \theta}
\end{aligned} \tag{19}$$

Substituting Eqs. (18) and (19) into Eq. (17) gives the stability equations in terms of the displacement components as

$$
\begin{gathered}
A_{11}\frac{\partial^2 u^1}{\partial x^2}+Q_{11}\frac{\partial^2 u^1}{R^2\partial\theta^2}+(A_{12}+Q_{11})\frac{\partial^2 v^1}{R\partial x\partial\theta}+A_{12}\frac{\partial w^1}{R\partial x}\\
-B_{11}\frac{\partial^3 w^1}{\partial x^3}-(B_{12}+2Q_{22})\frac{\partial^3 w^1}{R^2\partial x\partial\theta^2}=0\\
(A_{12}+Q_{11})\frac{\partial^2 u^1}{R\partial x\partial\theta}+Q_{11}\frac{\partial^2 v^1}{\partial x^2}+A_{11}\frac{\partial^2 v^1}{R^2\partial\theta^2}+A_{11}\frac{\partial w^1}{R^2\partial\theta}\\
-B_{11}\frac{\partial^3 w^1}{R^3\partial\theta^3}-(B_{12}+2Q_{22})\frac{\partial^3 w^1}{R\partial x^2\partial\theta}=0\\
B_{11}\frac{\partial^3 u^1}{\partial x^3}+(B_{12}+2Q_{22})\frac{\partial^3 u^1}{R^2\partial x\partial\theta^2}+(B_{12}+2Q_{22})\frac{\partial^3 v^1}{R\partial x^2\partial\theta}+B_{11}\frac{\partial^3 v^1}{R^3\partial\theta^3}\\
-A_{12}\frac{\partial u^1}{R\partial x}-A_{11}\left(\frac{\partial v^1}{R^2\partial\theta}+\frac{w^1}{R^2}\right)-D_{11}\frac{\partial^4 w^1}{\partial x^4}-D_{11}\frac{\partial^4 w^1}{R^4\partial\theta^4}\\
+B_{11}\frac{\partial^2 w^1}{R^3\partial\theta^2}-(D_{12}+4Q_{33})\frac{\partial^4 w^1}{R^2\partial x^2\partial\theta^2}+\left(\frac{B_{12}}{R}+\bar{N}_x^0\frac{B_{12}}{R^3}\right)\frac{\partial^2 w^1}{\partial x^2}=0
\end{gathered}
\tag{20}
$$

The cylindrical pipes are generally classified by referring to the type of support used in the absence of the body forces and lateral loads except the external temperature load. The boundary conditions are given by

$$
\frac{\partial u^1}{\partial x}=v^1=w^1=\frac{\partial^2 w^1}{\partial x^2}=0 \quad \text{at } x=0,L \tag{21}
$$

The following approximate solution satisfies the supported boundary conditions

$$
\begin{gathered}
u^1=\sum_{m=1}^{\infty}\sum_{n=1}^{\infty}U_{mn}^1\cos(\lambda x)\sin(\bar{n}\theta)\\
v^1=\sum_{m=1}^{\infty}\sum_{n=1}^{\infty}V_{mn}^1\sin(\lambda x)\cos(\bar{n}\theta)\\
w^1=\sum_{m=1}^{\infty}\sum_{n=1}^{\infty}W_{mn}^1\sin(\lambda x)\sin(\bar{n}\theta)
\end{gathered}
\tag{22}
$$

Where $0\le x\le L,\ 0\le\theta\le 2\pi,\ \lambda=m\pi/L,\ m$ and $\bar{n}$ are the number of half-waves in x- and θ-directions, respectively and U_{mn}^1, V_{mn}^1 and W_{mn}^1 are arbitrary parameters. Substituting Eq. (22) into Eq. (20), one obtains

$$
[C]\{\Lambda\}=0 \tag{23}
$$

where $\{\Lambda\}$ denotes the columns

$$
\{\Lambda\}=\{U^1, V^1, W^1\} \tag{24}
$$

The elements c_{ij} of the matrix $[C]$ are given by

$$
\begin{gathered}
c_{11}=A_{11}\lambda^2+A_{66}\left(\frac{\bar{n}}{R}\right)^2, \qquad c_{12}=(A_{12}+A_{66})\lambda\frac{\bar{n}}{R}\\
c_{21}=c_{12} \qquad c_{13}=-\frac{A_{12}}{R}\lambda-B_{11}\lambda^3-(B_{12}+B_{66})\lambda\left(\frac{\bar{n}}{R}\right)^2\\
c_{22}=A_{66}\lambda^2+A_{22}\left(\frac{\bar{n}}{R}\right)^2, \quad c_{23}=-A_{22}\frac{\bar{n}}{R^2}-B_{22}\left(\frac{\bar{n}}{R}\right)^3-(B_{12}+B_{66})\lambda^2\frac{\bar{n}}{R}\\
c_{31}=\frac{A_{12}}{R}\lambda+B_{11}\lambda^3+(B_{12}+2B_{66})\lambda\left(\frac{\bar{n}}{R}\right)^2\\
c_{32}=B_{22}\left(\frac{\bar{n}}{R}\right)^3+A_{22}\frac{\bar{n}}{R^2}+(B_{12}+2B_{66})\lambda^2\frac{\bar{n}}{R}\\
c_{33}=-D_{11}\lambda^4-2\frac{B_{12}}{R}\lambda^2-D_{22}\left(\frac{\bar{n}}{R}\right)^4-2B_{22}\frac{\bar{n}^2}{R^3}-2(D_{12}+D_{66})\lambda^2\left(\frac{\bar{n}}{R}\right)^2-\frac{A_{22}}{R^2}-\bar{N}_x^0\lambda^2
\end{gathered}
\tag{25}
$$

5. Thermal buckling solution

Consider functionally graded cylindrical pipe in which the temperature of the inner and outer surfaces of the cylindrical shell are T_a and T_b, respectively. The following presents the solution of the equation C=0 for different types of thermal loading conditions.

Uniform temperature rise.

The cylindrical pipe's initial temperature is assumed to be T_i. The temperature is uniformly raised to a final value T_f in which the cylindrical pipe buckles. The temperature change is

$$\Delta T = T_f - T_i \tag{26}$$

The critical buckling temperature difference is obtained by solving the determinant $|C| = 0$

$$\Delta T_{cr} = \frac{\eta+\mu}{\lambda^2\bar{\beta}_1} \tag{27}$$

Where

$$\eta = \frac{(c_{11}c_{23}c_{32} - c_{12}c_{23}c_{31} - c_{13}c_{21}c_{32} + c_{13}c_{22}c_{31})}{c_{11}c_{22} - c_{12}c_{21}} \tag{28}$$

$$\mu = D_{11}\lambda^4 + 2\frac{B_{12}}{R}\lambda^2 + D_{22}\left(\frac{\bar{n}}{R}\right)^4 + 2B_{22}\frac{\bar{n}^2}{R^3} + 2(D_{12}+D_{66})\lambda^2\left(\frac{\bar{n}}{R}\right)^2 + \frac{A_{22}}{R^2} \tag{29}$$

$$\bar{\beta}_1 = \int_{-h/2}^{h/2} \frac{\alpha^{(n)}(z)E^{(n)}(z)}{1-\upsilon}\,\mathrm{d}z \tag{30}$$

Non-Uniform temperature rise.

The temperature distribution is approximated linear through the thickness if the cylindrical pipe thickness is thin enough. Therefore, the temperature can be written as

$$\begin{gathered} T(z) = \Delta T\left(\frac{z}{h} + \frac{1}{2}\right) + T_m \\ \Delta T = T_p - T_m \end{gathered} \tag{31}$$

T_p is the temperature of the inner surface, and T_m is the temperature of the outer surface of a functionally graded shell The critical buckling temperature difference can be deduced as

$$\Delta T_{cr} = \frac{\eta+\mu}{\lambda^2\bar{\beta}_2} - \frac{T_a\bar{\beta}_1}{\bar{\beta}_2} \tag{32}$$

Where

$$\bar{\beta}_2 = \int_{-h/2}^{h/2} \frac{\alpha^{(n)}(z)E^{(n)}(z)}{1-\upsilon}\left(\frac{z}{h} + \frac{1}{2}\right)^{\gamma}\mathrm{d}z \tag{33}$$

For linear temperature, gamma is equal to unity, (γ=1).

6. Results

This section will present the results and discussion about the thermal buckling analysis of two new simply supported functionally graded cylindrical (FG-A and FG-B) pipe. The FGM cylindrical pipe is composed of a metal-ceramic mixture, specifically, a combination of Aluminum

Table 1 Effect of the inhomogeneity parameter “*N*” and the parameter “*h/R*” on the Critical buckling temperature difference ΔT_{cr} (*L/R*=1)

N	*h/R*	FG-A			FG-B		
		Linear	Uniform	Nonlinear ($\gamma = 2$)	Linear	Uniform	Nonlinear ($\gamma = 2$)
1	0.01	1184.30	617.17	1851.70	1262.60	656.20	1849.50
	0.02	1347.20	698.61	2106.40	1660.20	855.10	2431.30
	0.03	1618.70	834.35	2530.80	2322.90	1186.50	3401.80
	0.04	1998.80	1024.40	3125.10	3250.70	1650.40	4760.50
	0.05	2487.50	1268.70	3889.10	4443.60	2246.80	6507.40
	0.06	3084.70	1567.40	4822.90	5901.60	2975.80	8642.50
	0.07	3790.60	1920.30	5926.50	7624.70	3837.30	11166.00
	0.08	4605.00	2327.50	7199.80	9612.80	4831.40	14077.00
	0.09	5528.00	2789.00	8643.00	11866.00	5958.00	17377.00
	0.10	6559.70	3304.80	10256.00	14384.00	7217.20	21065.00
2	0.01	1213.70	631.84	1839.20	1233.30	641.62	1838.70
	0.02	1464.60	757.30	2219.40	1542.90	796.42	2300.30
	0.03	1882.80	966.40	2853.20	2058.90	1054.40	3069.70
	0.04	2468.30	1259.10	3740.40	2781.30	1415.60	4146.70
	0.05	3221.00	1635.50	4881.10	3710.10	1880.00	5531.50
	0.06	4141.10	2095.50	6275.30	4845.30	2447.60	7224.10
	0.07	5228.40	2639.20	7923.00	6186.90	3118.40	9224.30
	0.08	6482.90	3266.50	9824.10	7734.90	3892.40	11532.00
	0.09	7904.80	3977.40	11979.00	9489.30	4769.70	14148.00
	0.10	9493.90	4772.00	14387.00	11450.00	5750.10	17072.00
3	0.01	1219.10	634.56	1837.00	1227.80	638.91	1836.80
	0.02	1486.30	768.17	2239.60	1521.10	785.56	2275.50
	0.03	1931.70	990.85	2910.70	2010.00	1030.00	3006.80
	0.04	2555.20	1302.60	3850.20	2694.30	1372.20	4030.60
	0.05	3356.90	1703.40	5058.10	3574.20	1812.10	5346.90
	0.06	4336.70	2193.30	6534.50	4649.70	2349.80	6955.70
	0.07	5494.60	2772.30	8279.30	5920.60	2985.30	8857.00
	0.08	6830.70	3440.40	10292.00	7387.10	3718.60	11051.00
	0.09	8344.90	4197.50	12574.00	9049.20	4549.60	13537.00
	0.10	10037.00	5043.70	15124.00	10907.00	5478.40	16316.00

and Alumina ($E_m = 70$ Gpa, $\alpha_m = 23 \times 10^{-6}\ 1/°\mathrm{C}$, $E_c = 380$ Gpa, $\alpha_c = 7.4 \times 10^{-6}\ 1/°\mathrm{C}$). Poisson’s ratio ($\upsilon$) is assumed to be constant for both materials ($\upsilon_c = 0.3$). The pipe’s inner surface temperature (Ta) is set to a reference value of 25°C.

Numerical results illustrating the influence of various parameters on the critical buckling temperature difference are presented in Tables 1-4. These parameters include the inhomogeneity parameter (*N*), the radius ratio (*h/R*), the thickness ratio (*L/h*), and different types of temperature distributions. The data illustrates the interactions between these factors and their effects on buckling behavior, offering valuable insights for optimising design and material selection. For

Table 2 Effect of the inhomogeneity parameter "*N*" and the parameter "*L/h*" on the Critical buckling temperature difference ΔT_{cr} (*h/*R=0.05)

N	*L/R*	FG-A			FG-B		
		Linear	Uniform	Nonlinear ($\gamma = 2$)	Linear	Uniform	Nonlinear ($\gamma = 2$)
1	1.5	1210.40	630.18	1892.40	1286.80	668.38	1884.40
	2.0	1007.70	528.85	1575.50	1101.30	575.65	1612.80
	2.5	806.89	428.44	1261.60	928.01	489.00	1359.00
	3.0	659.13	354.56	1030.50	815.95	432.97	1194.90
	3.5	561.51	305.75	877.91	761.48	405.74	1115.20
	4.0	502.57	276.28	785.76	752.84	401.42	1102.50
	4.5	472.45	261.22	738.67	780.02	415.01	1142.30
	5.0	464.07	257.03	725.57	835.86	442.93	1224.10
2	1.5	1239.00	644.50	1877.60	1258.10	654.06	1875.80
	2.0	1042.80	546.40	1580.30	1066.20	558.10	1589.70
	2.5	852.31	451.15	1291.60	882.59	466.29	1315.90
	3.0	717.94	383.97	1088.00	757.14	403.57	1128.90
	3.5	636.50	343.25	964.54	686.49	368.24	1023.50
	4.0	596.42	323.21	903.81	658.99	354.49	982.52
	4.5	587.79	318.89	890.72	664.68	357.34	991.00
	5.0	603.49	326.74	914.52	696.44	373.22	1038.40
3	1.5	1244.30	647.16	1874.90	1252.80	651.40	1874.20
	2.0	1049.30	549.65	1581.10	1059.70	554.85	1585.30
	2.5	860.72	455.36	1296.90	874.18	462.09	1307.70
	3.0	728.83	389.41	1098.20	746.25	398.12	1116.40
	3.5	650.39	350.19	980.01	672.61	361.30	1006.20
	4.0	613.80	331.90	924.88	641.61	345.80	959.83
	4.5	609.15	329.57	917.86	643.32	346.66	962.39
	5.0	629.31	339.65	948.25	670.62	360.31	1003.20

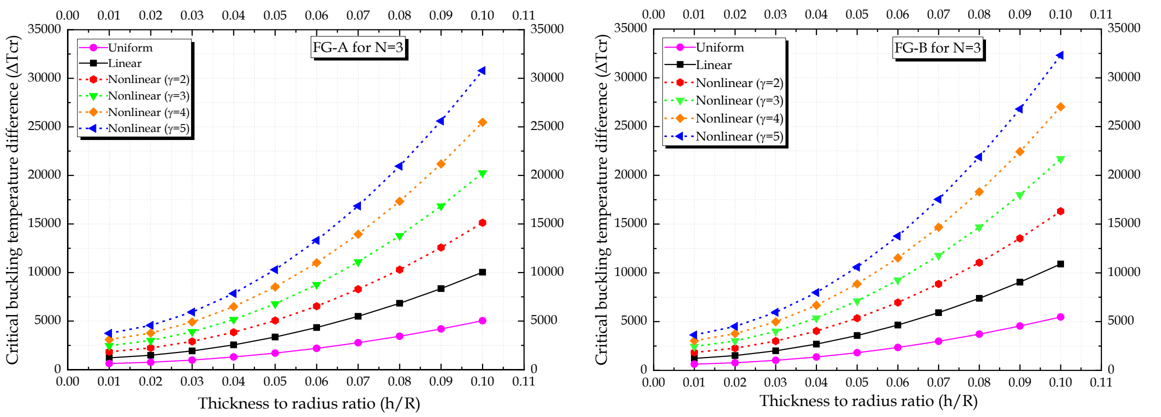

Fig. 3 Variation of the critical buckling temperature difference (ΔT_{cr}) according to the thickness ratio (h/R) of FG-A and FG-B shells

Table 3 Effect of the inhomogeneity parameter “*N*” and the parameter “*h/R*” on the Critical buckling temperature difference ΔT_{cr} with nonlinear temperature distribution (*L/R*=1)

N	h/R	FG-A				FG-B			
		$\gamma=2$	$\gamma=3$	$\gamma=4$	$\gamma=5$	$\gamma=2$	$\gamma=3$	$\gamma=4$	$\gamma=5$
1	0.01	1851.70	2578.00	3356.50	4183.00	1849.00	2408.20	2962.30	3522.80
	0.02	2106.40	2932.60	3818.10	4758.30	2431.30	3166.70	3895.20	4632.30
	0.03	2530.80	3523.50	4587.50	5717.10	3401.80	4430.70	5450.10	6481.30
	0.04	3125.10	4350.90	5664.60	7059.50	4760.50	6200.40	7627.00	9070.00
	0.05	3889.10	5414.60	7049.50	8785.40	6507.40	8475.60	10426.00	12398.00
	0.06	4822.90	6714.70	8742.20	10895.00	8642.50	11257.00	13846.00	16466.00
	0.07	5926.50	8251.10	10743.00	13388.00	11166.00	14543.00	17889.00	21274.00
	0.08	7199.80	10024.00	13051.00	16264.00	14077.00	18335.00	22554.00	26821.00
	0.09	8643.00	12033.00	15667.00	19524.00	17377.00	22633.00	27840.00	33108.00
	0.10	10256.00	14279.00	18590.00	23168.00	21065.00	27436.00	33749.00	40134.00
2	0.01	1839.20	2477.70	3136.90	3822.50	1838.70	2436.90	3024.80	3600.90
	0.02	2219.40	2989.90	3785.50	4612.80	2300.30	3048.70	3784.20	4504.80
	0.03	2853.20	3843.60	4866.30	5929.90	3069.70	4068.30	5049.80	6011.50
	0.04	3740.40	5038.80	6379.60	7773.90	4146.70	5495.80	6821.70	8120.70
	0.05	4881.10	6575.50	8325.10	10145.00	5531.50	7331.10	9099.80	10833.00
	0.06	6275.30	8453.70	10703.00	13042.00	7224.10	9574.30	11884.00	14147.00
	0.07	7923.00	10673.00	13513.00	16467.00	9224.30	12225.00	15175.00	18064.00
	0.08	9824.10	13235.00	16756.00	20418.00	11532.00	15284.00	18972.00	22584.00
	0.09	11979.00	16137.00	20431.00	24896.00	14148.00	18751.00	23275.00	27707.00
	0.10	14387.00	19381.00	24538.00	29901.00	17072.00	22626.00	28084.00	33432.00
3	0.01	1837.00	2460.50	3093.70	3739.30	1836.80	2442.50	3042.80	3636.50
	0.02	2239.60	2999.80	3771.80	4558.90	2275.50	3025.90	3769.60	4505.20
	0.03	2910.70	3898.60	4901.90	5924.90	3006.80	3998.30	4981.00	5952.90
	0.04	3850.20	5157.00	6484.10	7837.40	4030.60	5359.70	6677.00	7979.90
	0.05	5058.10	6774.90	8518.40	10296.00	5346.90	7110.10	8857.60	10586.00
	0.06	6534.50	8752.30	11005.00	13301.00	6955.70	9249.40	11523.00	13771.00
	0.07	8279.30	11089.00	13943.00	16853.00	8857.00	11778.00	14672.00	17535.00
	0.08	10292.00	13786.00	17334.00	20951.00	11051.00	14695.00	18307.00	21879.00
	0.09	12574.00	16842.00	21176.00	25596.00	13537.00	18001.00	22425.00	26801.00
	0.10	15124.00	20257.00	25471.00	30786.00	16316.00	21696.00	27029.00	32303.00

further details, the corresponding figures below have been plotted to represent these relationships and trends visually.

Fig. 3 represents the variation of the critical buckling temperature difference (ΔT_{cr}) according to the thickness ratio (*h*/*R*) of FG-A and FG-B shells. The figure also explores the impact of various thermal loadings, “uniform”, “linear” and “nonlinear” with γ values of 2. 3. 4. and 5.

As depicted in Fig. 3. the influence of thickness ratio (*h/R*) on ΔT_{cr} is highlighted. Illustrating an expected rise in ΔT_{cr} with increasing *h/R*. Indicating that thicker shells can withstand higher temperature increases before buckling. Furthermore. it examines how the inhomogeneity parameter (uniform. linear. nonlinear) affects ΔT_{cr}. The nonlinear case may exhibit the lowest ΔT_{cr}

Table 4 Effect of the inhomogeneity parameter "*N*" and the parameter "*L/h*" on the Critical buckling temperature difference ΔT_{cr} with nonlinear temperature distribution (*h/R*=0.05)

N	*h/R*	FG-A				FG-B			
		$\gamma=2$	$\gamma=3$	$\gamma=4$	$\gamma=5$	$\gamma=2$	$\gamma=3$	$\gamma=4$	$\gamma=5$
1	1.5	1892.40	2634.70	3430.20	4274.90	1884.40	2454.30	3019.00	3590.30
	2.0	1575.50	2193.60	2855.90	3559.10	1612.80	2100.60	2583.90	3072.80
	2.5	1261.60	1756.40	2286.80	2849.90	1359.00	1770.10	2177.30	2589.30
	3.0	1030.50	1434.80	1868.00	2328.00	1194.90	1556.30	1914.40	2276.60
	3.5	877.91	1222.30	1591.40	1983.20	1115.20	1452.40	1786.60	2124.70
	4.0	785.76	1094.00	1424.30	1775.00	1102.50	1436.00	1766.30	2100.50
	4.5	738.67	1028.40	1338.90	1668.70	1142.30	1487.80	1830.10	2176.40
	5.0	725.57	1010.20	1315.20	1639.10	1224.10	1594.30	1961.10	2332.20
2	1.5	1877.60	2529.40	3202.40	3902.30	1875.80	2486.10	3085.80	3673.50
	2.0	1580.30	2128.80	2695.30	3284.40	1589.70	2106.80	2615.10	3113.10
	2.5	1291.60	1739.90	2202.90	2684.40	1315.90	1744.00	2164.80	2577.00
	3.0	1088.00	1465.60	1855.60	2261.20	1128.90	1496.10	1857.10	2210.70
	3.5	964.54	1299.40	1645.10	2004.70	1023.50	1356.50	1683.80	2004.40
	4.0	903.81	1217.60	1541.50	1878.50	982.52	1302.20	1616.30	1924.10
	4.5	890.72	1199.90	1519.20	1851.30	991.00	1313.40	1630.30	1940.70
	5.0	914.52	1232.00	1559.80	1900.70	1038.40	1376.20	1708.20	2033.50
3	1.5	1874.90	2511.30	3157.60	3816.60	1874.20	2492.20	3104.70	3710.50
	2.0	1581.10	2117.70	2662.80	3218.50	1585.30	2108.10	2626.20	3138.60
	2.5	1296.90	1737.10	2184.20	2640.00	1307.70	1739.00	2166.40	2589.10
	3.0	1098.20	1470.90	1849.50	2235.50	1116.40	1484.50	1849.40	2210.20
	3.5	980.01	1312.60	1650.40	1994.90	1006.20	1338.00	1666.90	1992.10
	4.0	924.88	1238.80	1557.60	1882.70	959.83	1276.30	1590.00	1900.30
	4.5	917.86	1229.40	1545.80	1868.40	962.39	1279.70	1594.30	1905.40
	5.0	948.25	1270.10	1597.00	1930.20	1003.20	1334.10	1661.90	1986.20

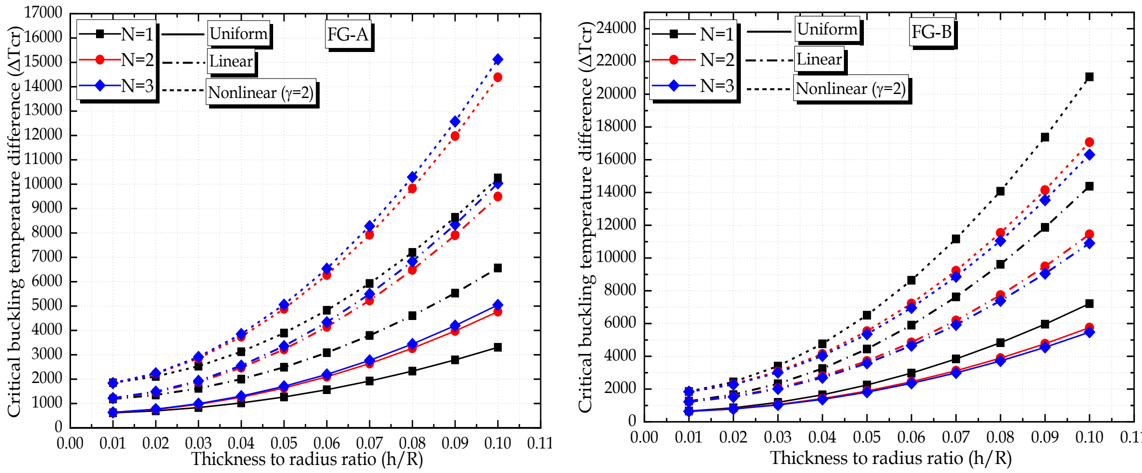

Fig. 4 Critical buckling temperature difference (ΔT_{cr}) against the thickness ratio (*h/R*) for various inhomogeneity parameter "*N*" values

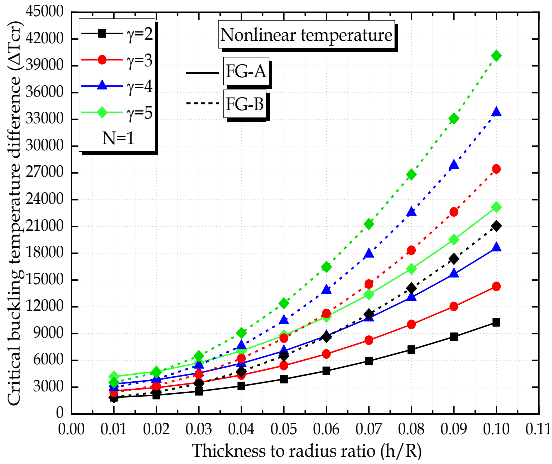

Fig. 5 Critical buckling temperature difference (ΔT_{cr}) plotted against the thickness ratio (h/R) for different nonlinear temperature distribution parameter

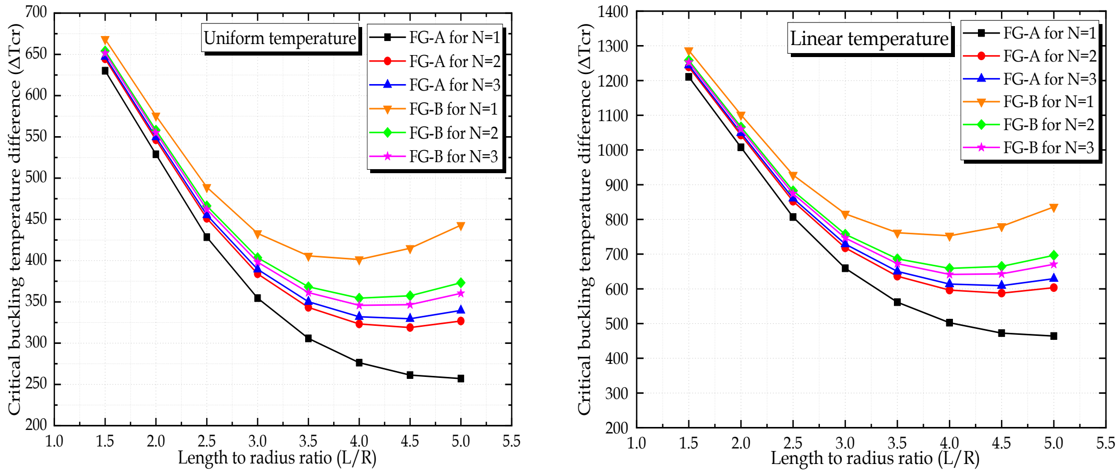

(a) Uniform (b) Linear

Fig. 6 Critical buckling temperature difference (ΔT_{cr}) plotted against the length ratio (L/R) for different values of the inhomogeneity parameter

due to its less uniform material distribution. Potentially leading to earlier buckling under thermal stress. Additionally. it explores the distinct ΔT_{cr} behaviors of FG-A and FG-B materials. reflecting their differing material properties.

Fig. 4 shows the evolution of the critical temperature difference with the thickness ratio (h/R) for FG-A and FG-B shells. Demonstrating an anticipated increase in ΔT_{cr} as h/R increases. Indicatingmore significant resistance to thermal buckling in thicker shells. It also explores a specific inhomogeneity parameter value. Allowing for a detailed comparison of how the material distribution parameter (N) influences the behavior of FG-A and FG-B. The figure presents distinct curves for N=1, 2, and 3. Suggesting a potential trend where ΔT_{cr} rises with an increasing parameter (N), potentially due to improved load distribution across the shell thickness.

Fig. 5 provides a detailed analysis of the critical buckling temperature difference (ΔT_{cr}) for FG-A and FG-B cylindrical shells. Highlighting the impact of the nonlinear temperature distribution parameter (γ) and thickness ratio (*h/R*). It shows that as both γ and *h/R* increase. ΔT_{cr} also increases. Indicating that shells with higher nonlinear temperature gradients and thickness ratios can withstand greater temperature increases before buckling occurs.

Fig. 6 illustrates the relationship between the critical buckling temperature difference (ΔT_{cr}) and the length-to-radius ratio (*L/R*) of FG-A and FG-B cylinders under different thermal loading conditions. It can be observed that generally. Increasing the length-to-radius ratio (*L/R*) decreases the critical buckling temperature difference (ΔT_{cr}).

7. Conclusions

In this paper, the thermal buckling behavior of novel functionally graded (FG) cylindrical pipes is investigated. Two newly introduced cosine function-based FG models, FG-A and FG-B, are used. The material properties and thermal expansion coefficients are assumed to vary continuously through the thickness. Equilibrium and stability equations for FG cylindrical pipes with supported boundary conditions are derived using Donnell's theory. The influence of geometrical aspects and inhomogeneity parameters (gradient index) on the critical buckling temperature of various functionally graded cylindrical structures is also examined. Thermal loads are assumed to vary uniformly, linearly, and nonlinearly through the thickness direction. Accurate and simplified formulas are provided for each temperature rise case, with exact and approximate formulations for different scenarios. The following conclusions can be drawn from the results:

- The effect of the thickness-to-radius ratio (*h/R*) on critical buckling temperature difference illustrates that ΔT_{cr} is expected rised with increasing *h/R*. Indicating that thicker shells can withstand higher temperature increases before buckling.
- The inhomogeneity parameter (uniform, linear, or nonlinear) affects ΔT_{cr}. Results show that the nonlinear case may exhibit the lowest ΔT_{cr} due to its less uniform material distribution, which may lead to earlier buckling under thermal stress. Additionally, it explores the distinct ΔT_{cr} behaviors of FG-A and FG-B materials, reflecting their dissimilar material properties.
- The critical buckling temperature difference for FG-A and FG-B cylindrical shells. Highlight the impact of the nonlinear temperature distribution parameter (γ) and thickness-to-radius ratio (*h/R*).
- The results show that the critical buckling temperature difference ΔT_{cr} increases with the increase of γ and *h/R* values. Indicating that shells with higher nonlinear temperature gradients and thickness ratios can withstand more significant temperature increases prior to buckling.
- The relationship between the critical buckling temperature difference and the length-to-radius ratio of FG-A and FG-B cylinders under different thermal loading conditions reveals that increasing the length-to-radius ratio decreases the critical buckling temperature difference.

References

Belarbi, M.O., Benounas, S., Salami, S.J., Khechai, A., Daikh, A.A., Houari, M.S.A. and Bezzina, S. (2025), "An enhanced finite element model for static bending analysis of functionally graded plates with power-law, exponential, and sigmoid material gradients", *Arch. Appl. Mech.*, **95**(1), 1-24.

https://doi.org/10.1007/s00419-024-02727-x.
Bezzina, S., Bessaim, A., Houari, M.S.A. and Azab, M. (2022), “A new quasi-3D plate theory for free vibration analysis of advanced composite nanoplates”, *Steel Compos. Struct.*, **45**(6), 830-850. https://doi.org/10.12989/sss.2022.45.6.839.
Bhangale, R.K., Ganesan, N. and Padmanabhan, C. (2006), “Linear thermoelastic buckling and free vibration behavior of functionally graded truncated conical shells”, *J. Sound Vib.*, **292**(1-2), 341-371. https://doi.org/10.1016/j.jsv.2005.07.039.
Chen, W.R., Chen, C.S. and Chang, H. (2020), “Thermal buckling analysis of functionally graded Euler-Bernoulli beams with temperature-dependent properties”, *J. Appl. Comput. Mech.*, **6**(3), 457-470. https://doi.org/10.22055/jacm.2019.30449.1734.
Čukanović, D.V., Bogdanović, G.M., Radaković, A.B., Milosavljević, D.I., Veljović, L.V. and Balać, I.M. (2017), “Comparative thermal buckling analysis of functionally graded plate”, *Therm. Sci.*, **21**(6 Part B), 2957-2969. https://doi.org/10.2298/TSCI160614182C.
Daikh, A.A., Bachiri, A., Houari, M.S.A. and Tounsi, A. (2022), “Size dependent free vibration and buckling of multilayered carbon nanotubes reinforced composite nanoplates in thermal environment”, *Mech. Bas. Des. Struct. Mach.*, **50**(4), 1371-1399. https://doi.org/10.1080/15397734.2020.1752232.
Daikh, A.A., Belarbi, M.O., Ahmed, D., Houari, M.S.A., Avcar, M., Tounsi, A. and Eltaher, M.A. (2023), “Static analysis of functionally graded plate structures resting on variable elastic foundation under various boundary conditions”, *Acta Mechanica*, **234**(2), 775-806. https://doi.org/10.1007/s00707-022-03405-1.
Daikh, A.A., Belarbi, M.O., Vinh, P.V., Ladmek, M., Belkacem, A., Houari, M.S.A., ... & Eltaher, M.A. (2024), “An assessment of a new hyperbolic shear deformation theory for the free vibration analysis of cosine functionally graded doubly curved shells under various boundary conditions”, *Phys. Mesomech.*, **27**(3), 338-354. https://doi.org/10.1134/S102995992403010X.
Elmascri, S., Bessaim, A., Taleb, O., Houari, M.S.A., Mohamed, S., Bernard, F. and Tounsi, A. (2020), “A novel hyperbolic plate theory including stretching effect for free vibration analysis of advanced composite plates in thermal environments”, *Struct. Eng. Mech.*, **75**(2), 193-209. https://doi.org/10.12989/sem.2020.75.2.193.
Farhatnia, F., Ghanbari-Mobarakeh, M., Rasouli-Jazi, S. and Oveissi, S. (2017), “Thermal buckling analysis of functionally graded circular plate resting on the Pasternak elastic foundation via the differential transform method”, *Facta Universitatis, Ser.: Mech. Eng.*, **15**(3), 545-563. https://doi.org/10.22190/FUME170104004F.
Gupta, A.K. and Kumar, A. (2023), “Buckling analysis of porous functionally graded plates”, *Eng. Technol. Appl. Sci. Res.*, **13**(3), 10901-10905.
Ibrahimbegovic, A., Hajdo, E. and Dolarevic, S. (2013), “Linear instability or buckling problems for mechanical and coupled thermomechanical extreme conditions”, *Couple. Syst. Mech.*, **2**(4), 349-374. https://doi.org/10.12989/csm.2013.2.4.349.
Khayat, M., Poorveis, D. and Moradi, S. (2017), “Buckling analysis of functionally graded truncated conical shells under external displacement-dependent pressure”, *Steel Compos. Struct.*, **23**(1), 1-16. https://doi.org/10.1016/j.tws.2008.05.006.
Lanhe, W., Hongjun, W. and Daobin, W. (2007), “Dynamic stability analysis of FGM plates by the moving least squares differential quadrature method”, *Compos. Struct.*, **77**(3), 383-394. https://doi.org/10.1016/j.compstruct.2005.07.011.
Li, D., Zhu, H. and Gong, X. (2021), “Buckling analysis of functionally graded sandwich plates under both mechanical and thermal loads”, *Mater.*, **14**(23), 7194. https://doi.org/10.3390/ma14237194.
Maknun, I.J. and Annisa, B. (2024), “Mechanical and thermal buckling analysis of functionally graded material (FGM) plate using triangular element”, *AIP Conf. Proc.*, **3074**(1), 020016. https://doi.org/10.1063/5.0211563.
Mohammadi, M., Rajabi, M. and Ghadiri, M. (2021), “Functionally graded materials (FGMs): A review of classifications, fabrication methods and their applications”, *Proc. Appl. Ceram.*, **15**(4), 319-343. https://doi.org/10.2298/PAC2104319M.
Mokhefi, D., Bessaim, A., Houari, M.S.A., Deffane, Z., Houari-Belkadi, H., Ali, B., ... & Merzouki, T.

(2024), “A nonlocal strain gradient model for buckling analysis of advanced FG CNT-reinforced composite nanobeams”, *Couple. Syst. Mech.*, **13**(5), 375-393. https://doi.org/10.12989/csm.2024.13.5.375.
Ngo, V.M., Ibrahimbegovic, A. and Hajdo, E. (2014), “Nonlinear instability problems including localized plastic failure and large deformations for extreme thermo-mechanical loads”, *Couple. Syst. Mech.*, **3**(1), 89-110. https://doi.org/10.12989/csm.2014.3.1.089.
Oyekoya, O.O., Mba, D.U. and El-Zafrany, A.M. (2009), “Buckling and vibration analysis of functionally graded composite structures using the finite element method”, *Compos. Struct.*, **89**(1), 134-142. https://doi.org/10.1016/j.compstruct.2008.07.022.
Park, J.S. and Kim, J.H. (2006), “Thermal postbuckling and vibration analyses of functionally graded plates”, *J. Sound Vib.*, **289**(1-2), 77-93. https://doi.org/10.1016/j.jsv.2005.01.031.
Radaković, A., Čukanović, D., Bogdanović, G., Blagojević, M., Stojanović, B., Dragović, D. and Manić, N. (2020), “Thermal buckling and free vibration analysis of functionally graded plate resting on an elastic foundation according to high order shear deformation theory based on new shape function”, *Appl. Sci.*, **10**(12), 4190. https://doi.org/10.3390/app10124190.
Sepiani, H.A., Rastgoo, A., Ebrahimi, F. and Arani, A.G. (2010), “Vibration and buckling analysis of two-layered functionally graded cylindrical shell, considering the effects of transverse shear and rotary inertia”, *Mater. Des.*, **31**(3), 1063-1069. https://doi.org/10.1016/j.matdes.2009.09.052.
Shen, H.S. (2007), “Thermal postbuckling behavior of shear deformable FGM plates with temperature-dependent properties”, *Int. J. Mech. Sci.*, **49**(4), 466-478. https://doi.org/10.1016/j.ijmecsci.2006.09.011.
Shen, H.S. (2009), “Torsional buckling and postbuckling of FGM cylindrical shells in thermal environments”, *Int. J. Nonlin. Mech.*, **44**(6), 644-657. https://doi.org/10.1016/j.ijnonlinmec.2009.02.009.
Sofiyev, A.H. (2009), “The vibration and stability behavior of freely supported FGM conical shells subjected to external pressure”, *Compos. Struct.*, **89**(3), 356-366. https://doi.org/10.1016/j.compstruct.2008.08.010.
Sofiyev, A.H. (2010), “The buckling of FGM truncated conical shells subjected to axial compressive load and resting on Winkler–Pasternak foundations”, *Int. J. Press. Ves. Pip.*, **87**(12), 753-761. https://doi.org/10.1016/j.ijpvp.2010.08.012.
Sofiyev, A.H., Zerin, Z. and Korkmaz, A. (2008), “The stability of a thin three-layered composite truncated conical shell containing an FGM layer subjected to non-uniform lateral pressure”, *Compos. Struct.*, **85**(2), 105-115. https://doi.org/10.1016/j.compstruct.2007.10.022.
Van Do, T., Hong Doan, D., Chi Tho, N. and Dinh Duc, N. (2022), “Thermal buckling analysis of cracked functionally graded plates”, *Int. J. Struct. Stab. Dyn.*, **22**(08), 2250089. https://doi.org/10.1142/S0219455422500894.
Wei, Y.Y., Al-Furjan, M.S.H., Shan, L., Shen, X., Kolahchi, R., Rabani Bidgoli, M. and Farrokhian, A. (2024), “Micro-mass sensor-based vibration response of smart bidirectional functionally graded auxetic microbeams”, *Arch. Civil Mech. Eng.*, **24**(1), 38. https://doi.org/10.1007/s43452-023-00840-2.
Zamani Nejad, M., Jabbari, M. and Hadi, A. (2017), “A review of functionally graded thick cylindrical and conical shells”, *J. Comput. Appl. Mech.*, **48**(2), 357-370. https://doi.org/10.22059/JCAMECH.2017.247963.220.
Zhang, J., Chen, S. and Zheng, W. (2020), “Dynamic buckling analysis of functionally graded material cylindrical shells under thermal shock”, *Continuum Mech. Thermodyn.*, **32**, 1095-1108. https://doi.org/10.1007/s00161-019-00812-z.